ASTRONOMY AND SPACE SCIENCE
eds. M.K. Tsvetkov, L.G. Filipov, M.S. Dimitrijević, L.Č. Popović,
Heron Press Ltd, Sofia 2007

Microlensing in the X-Ray Band of Lensed QSOs

P. Jovanović[1], **L.Č. Popović**

Astronomical Observatory Belgrade, Volina 7, 11160 Belgrade, Serbia

Abstract. We investigate the influence of gravitational microlensing on detected X-ray radiation from three lensed quasars: MG J0414+0534, QSO 2237+0305 and H1413+117. The focus is set to the analysis of the Fe Kα spectral line and X-ray continuum variations due to gravitational microlensing. The accretion disk emission is analyzed by numerical simulations, based on a ray-tracing method in a Kerr metric, taking into account only photon trajectories reaching the observer's sky plane. Obtained results show that microlensing can satisfactorily explain the observed excess in the iron line emission in the case of the analyzed gravitational lens systems.

1 Introduction

Recent observational and theoretical studies suggest that gravitational microlensing can induce variability in the X-ray emission of lensed QSOs. Microlensing of the Fe Kα line has been reported at least in three macrolensed QSOs: MG J0414+0534 [1], QSO 2237+0305 [2], and H1413+117 [3–5]. The observed enhancement of the Fe Kα line in these three gravitationally lensed QSOs was not followed by an equivalent X-ray continuum amplification.

An explanation for different behavior of the line and continuum variability in the observed events should be given in context of the microlensing hypothesis. An increase of the Fe Kα equivalent width in the image B of the lensed QSO J0414+0534 that was not followed by the continuum, was explained by proposing that the thermal emission region of the disk and the Compton up-scattered emission region of the hard X-ray source lie within a smaller radius than the iron-line reprocessing region [1]. An amplification of the Fe Kα line in component A of QSO 2237+0305 was measured but also not in the continuum [2]. However, in this case the authors gave diffrent interpretation, suggesting that the larger size of the continuum emission region ($\sim 10^{14}$ cm $\sim$ 100 R_g for $M_{BH} = 10^7 M_\odot$) with respect to the Fe Kα emission region ($\sim$ 10 R_g) could explain this result [2]. Finally, in the case of H 1413+117 it was found that the continuum and the Fe Kα line were enhanced by a different factor [3].

With the aim of discussing these results, we will model here the behavior of the

X-ray continuum and the Fe Kα line during a microlensing event for different sizes of the continuum and the Fe Kα line emission regions.

2 Microlensing of a Compact Accretion Disk

The assumption of a disk geometry for the distribution of Fe Kα emitters is supported by the spectral shape of this line in AGN (e.g. [6], where they have investigated iron line properties of 18 Sy 1 galaxies). Regarding the X-ray continuum emission, it seems that it mainly arises from an accretion disk. For instance, it was shown in [7] that the X-ray spectral variability of MCG-6-30-15 can be modeled by a two-component model where the one, varying component, is a power-law and the other constant component is produced by very strong reflection from a relativistic disk.

To study the effects of microlensing on a compact accretion disk we will use the ray tracing method considering only those photon trajectories that reach the sky plane at a given observer's angle $\theta_{\rm obs}$ (see e.g. [5, 8] and references therein). According to [9], the amplified brightness with amplification $A(X,Y)$ for the continuum is given by:

$$I_C(X,Y;E_{obs}) = I_P(E_{obs}, T(X,Y)) \cdot A(X,Y), \tag{1}$$

and for the Fe Kα line by

$$\begin{aligned} I_L(X,Y;E_{obs}) = \quad & I_P(E_0 \cdot g(X,Y), T(X,Y)) \cdot \\ & \delta(E_{obs} - E_0 \cdot g(X,Y)) \cdot A(X,Y), \end{aligned} \tag{2}$$

where $T(X,Y)$ is the temperature, X and Y are the impact parameters which describe the apparent position of each point of the accretion disk image on the celestial sphere as seen by an observer at infinity; E_0 is the the line transition energy ($E_0^{\rm Fe\ K\alpha} = 6.4$ keV) and $g(X,Y) = E_{\rm obs}/E_{\rm em}$ is the energy shift due to relativistic effects ($E_{\rm obs}$ is the observed energy and $E_{\rm em}$ is the emitted energy from the disk). Here we will not consider the cosmological redshift.

The emissivity of the disk is one of the important parameters which has influence on the continuum and line shapes. The observed continuum flux is very often fitted with one or two black-body components in the soft X-ray, in addition to the hard X-ray power law (see e.g. [10]). The line shape, as well as the continuum distribution, strongly depend on an assumption for emissivity law. In the standard Shakura-Sunyaev disk model [11], accretion occurs via an optically thick and geometrically thin disk. The effective optical depth in the disk is very high and photons are close to thermal equilibrium with electrons. The surface temperature is a function of disk parameters and results in the multicolor black body spectrum. This component is thought to explain the 'blue bump' in AGN and the soft X-ray emission in galactic black holes. Although the standard model

does not predict the power-law X-ray emission observed in all sub-Eddington accreting black holes, the power law for the X-ray emissivity in AGN is usually accepted (see e.g. [12]). But one can not exclude other emissivity laws, such as black-body or modified black-body emissivity laws. Therefore, we will use here black-body, modified black-body and power emissivity laws for both; the Fe Kα and continuum emission.

In the case of the black-body radiation law, the disk emissivity is given as (e.g. [13]):

$$I_P(X,Y;E) = B[E, T_s(X,Y)], \tag{3}$$

where

$$B\left(E, T_s(X,Y)\right) = \frac{2E^3}{h^2c^2}\frac{1}{e^{E/kT_s(X,Y)}-1}, \tag{4}$$

where c is the speed of light, h is the Planck constant, k is the Boltzmann constant and $T_s(X,Y)$ is the surface temperature of X-ray accretion disk.

In principle, one can assume different distribution of the surface temperature along disk. To obtained the X-ray continuum distribution using Eq. (4) one can assume that $T_s = const.$, taking that the black hole is powerful X-ray sources with an effective temperature 10^7 to 10^8 K. But, regarding the standard disk model it is expected that the surface temperature at least is radially dependent. Therefore, here we will accept the radial distribution of surface temperature given by [11]:

$$T_s(X,Y) \sim r^{-3/2}(X,Y)(1-r^{-1/2}(X,Y))^{4/5}\,\mathrm{K}, \tag{5}$$

taking that an effective temperature is in an interval from 10^7 to 10^8 K. The distribution of the temperature along the radius of the disk used in this paper is given in Figure 1 (top) and corresponding shape of spectral energy distribution is shown in Figure 1 (bottom). In Eq. (4) r is the dimensionless parameter defined as:

$$r(X,Y) = \frac{R(X,Y)}{6R_g} = \frac{1}{6}\frac{R(X,Y)c^2}{GM} = \frac{M_\odot}{M}\frac{R(X,Y)}{9\ \mathrm{km}}, \tag{6}$$

where $R(X,Y)$ is disk radius, expressed in gravitational radii R_g.

However, in the innermost part of the accretion disk the Planck function cannot be used properly. Therefore we will use also the standard (classical) Shakura – Sunyaev approach, where the emissivity law is described by a "modified" black-body radiation law (Eqs. (3.4), (3.8) in [11])

$$I_P(E;X,Y) \propto x^3\exp(-x), \tag{7}$$

where $x = E/kT(X,Y)$. Taking into account that the observed hard X-ray continuum has a power-law type spectral shape, we will also assume that the time-independent intrinsic emissivity of the continuum is:

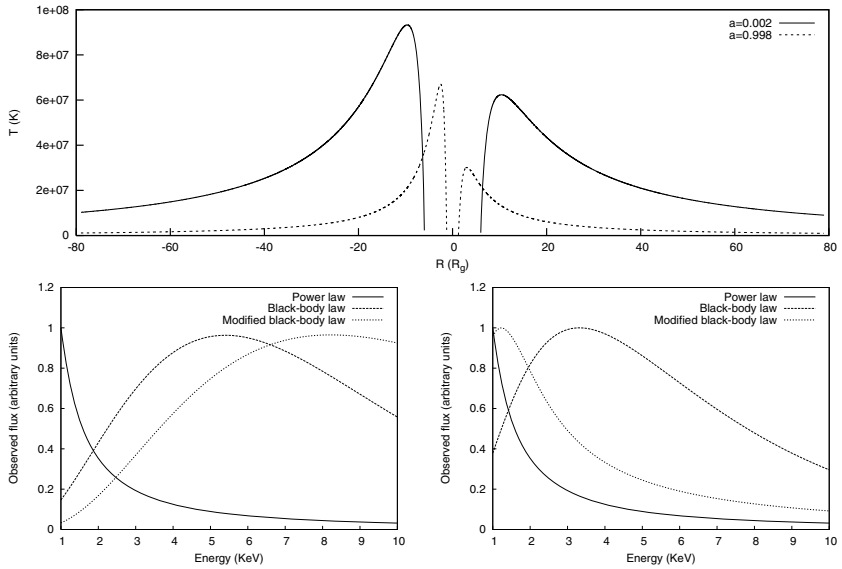

Figure 1. Top: The distribution of the temperature as a function of the radius along the direction of the disk rotation, given for two diferent values of angular momentum a. Negative values of R correspond to the approaching and positive values to the receiding side of the disk. Bottom: Shapes of the contunuum for considered three emissivity laws (normalized to the maximal value) for an accretion disk with outher radius of 20 R_g (left) and 80 R_g (right).

$$I(E,r) \sim E^{-\Gamma} \times r^{-\alpha}, \tag{8}$$

where, according to the investigation of observed X-ray spectra, Γ and α are taken to be 1.5 and 2.5 (see e.g. [14]). For the Fe Kα emission in this case we used the same calculation as in [5, 15].

We should note here, that disk may be considered to be composed of a number of distinct parts with different physical conditions (e.g. radiation pressure dominant part, matter pressure dominant part, etc. see e.g. [11]). Consequently, in general one can expect that the disk can be described by different emissivity laws in different parts (e.g. the black-body law may be applied in outer part of the disk). Taking into account a huge number of parameters which should be considered in the case of microlensed disk (see the next section), we will consider only one emissivity law for whole disk.

The total observed flux for the continuum and the Fe Kα line is given as [9]:

$$F(E) = \int_{\text{image}} [I_C(X,Y;E) + I_L(X,Y;E)] d\Omega, \tag{9}$$

where $d\Omega$ is the solid angle subtended by the disk in the observer's sky and the integral extends over the whole emitting region.

As one can see from Eq. (9) the total observed flux is a sum of the continuum and the line fluxes, consequently, the amplification in the continuum and in the Fe Kα line can be considered separately as two independent components. On the other hand, the amplifications will depend on the sizes and geometry of the continuum and line emitting regions. In further text we will consider amplifications in the line and in the continuum separately.

2.1 Accretion disk parameters

For the disk inclination we adopt the averaged values given in [6] from the study of the Fe Kα line profiles of 18 Seyfert 1 galaxies: $i = 35^{\circ}$. The inner radius, R_{in}, can not be smaller than the radius of the marginally stable orbit, R_{ms}, that corresponds to $R_{ms} = 6R_g$ (gravitational radii, $R_g = GM/c^2$, where G is gravitational constant, M is the mass of central black hole, and c is the velocity of light) in the Schwarzschild metric and to $R_{ms} = 1.23R_g$ in the case of the Kerr metric with angular momentum parameter $a = 0.998$. To select the outer radius, R_{out}, we take into account previous investigations of the X-ray variability that support very compact X-ray emitting disks (e.g. $\sim 3 \times 10^{14}\mathrm{cm}$ for the X-ray continuum emission region of lensed blazar PKS 1830-211 [16]). So, considering a range of black hole masses of $10^7 - 10^9$ $\mathrm{M}_{\odot}$ we can conclude that the X-ray emission is coming from a compact region of the order of 10 to 100 R_g. This range of sizes is also acceptable for the Fe Kα emission region (see e.g. [6, 12]). We adopt the central black hole mass from [17]: $M_8 = 10^8 M_{\odot}$.

It is difficult to discuss the validity of different emissivity laws for demonstration of the X-ray emission (in the line as well as in the continuum), but sometimes, as for example in the case of black-body emissivity law, the emissivity at X-ray wavelengths can be extremely small compared with, for example, optical wavelengths, and X-ray photons are emitted from a quite small region. In Figure 1 (bottom), we presented the continuum shapes for different emissivity laws used in the calculation (maximum of each is normalized to one). The shapes of the continuum were calculated for different dimensions of the disk. As one can see from Figure 1 (bottom), the shape of the continuum strongly depends not only on emissivity law, but also on disk dimensions.

2.2 Microlens model and parameters

Different types of caustics can be used to explain the observed microlensing events in quasars. Moreover, for an exact event one can model the caustic shape to obtain different parameters (see e.g. [18, 19] for the case of QSO 2237+0305). In order to apply an appropriate microlens model, we will consider a standard microlensing magnification pattern (Figure 2, left) for the QSO 2237+0305A

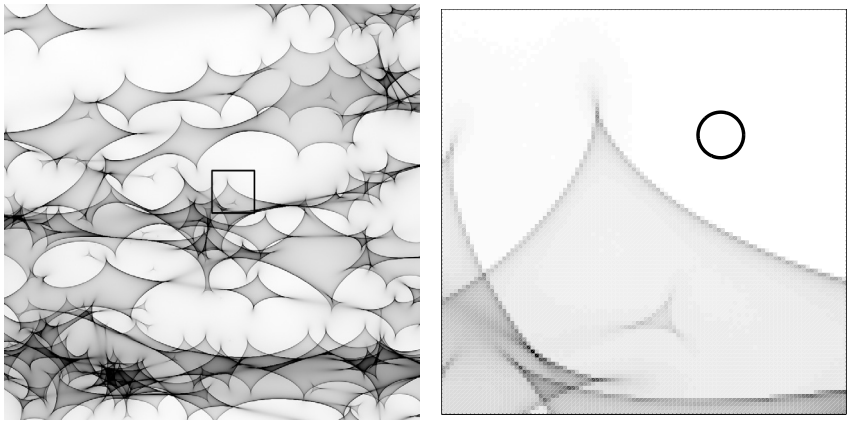

Figure 2. *Left:* microlensing map of QSO 2237+0305A image with 16 ERR (177372 R_g) on a side [18]. *Right:* the small part (square in Figure left) of the microlensing pattern, compared to a face-on accretion disk [9]. The assumed outer radius of the disk is $R_{out} = 1000\ R_g$.

image with 16 Einstein ring radii (ERR) on a side and $\kappa = 0.36$, $\lambda = 0.40$ and $\kappa_c = 0$. The mass of microlens is taken to be $1 M_\odot$. The simulation was made employing ray-shooting techniques that send rays from the observer through the lens to the source plane (see e.g. [20–23]). We assume a flat cosmological model with $\Omega = 0.3$ and $H_o = 70\ \mathrm{km\ s^{-1} Mpc^{-1}}$.

In Figure 2 we presented a comparison between the projected magnification map in the source plane and an accretion disk with a size of 1000 R_g (presented as a circle in Figure 2, right).

3 Results and Discussion

In Table 1 we give the Einstein Ring Radii (ERR) for the lensed QSOs where amplification of the Fe Kα line has been observed (MG J0414+0534, [1]; QSO H1413+117, [3, 4] and QSO 2237+0305, [2]). The ERRs (expressed in gravitational radii) are computed for different deflector masses and for a black hole mass of $10^8\ M_\odot$. We found that even deflectors with small mass have ERR with sizes from several tens to several hundreds of gravitational radii.

Here we consider a situation where a low mass population of microlenses (smaller than one solar mass) can form pattern structures (see Table 1) which are comparable with the size of the X-ray accretion disk. Moreover, the black hole mass of the lensed quasar may be of the order of $10^{9-10} M_\odot$, taking that $R_g \sim M_{BH}$, the pattern structure of low mass microlenses are comparable with a X-ray disk size of several dozens R_g. Therefore, here we consider that the black hole mass of the lensed quasar is $10^9 M_\odot$.

Table 1. ERR (expressed in gravitational radii) for different deflector masses (in $M_\odot$) for the three lensed QSOs where microlensing of the Fe Kα line is suspected [9]: J0414+0534 - [1], QSO H1413+117 - [3, 4], QSO 2237+0305 - [2]. Used values for the cosmological constants are: $H_0 = 50$ km s^{-1}Mpc^{-1} and $\Omega_0 = 1$. The black hole mass is assumed to be $10^8 M_\odot$.

Object	z_s	z_l	1×10^{-4}	1×10^{-3}	1×10^{-2}	1×10^{-1}	1
MG J0414+0534	2.64	0.96	20.3	64.2	203.1	642.3	2031.1
QSO 2237+0305	1.69	0.04	11.2	35.4	112.1	354.5	1121.0
QSO H1413+117	2.56	1.00	19.8	62.5	197.7	625.2	1977.0

For modeling of the caustic magnification pattern for image QSO 2237+0305A we used the same values for the convergence and external shear as presented in Figure 2, but for a low mass population, taking that the mass of the deflectors are randomly distributed in an interval ranging from 0.1 $M_\odot$ to 0.6 $M_\odot$, with a mean value of $< m >= 0.35\ M_\odot$. Also, the positions of the lenses were distributed randomly in a rectangular region in the lens plane, significantly larger than the considered region in the source plane. Taking the mean deflector mass as $< m >= 0.35\ M_\odot$ and $R_g = 9.547.10^{-6} M_{BH}/M_8$ pc, we modeled a caustic magnification pattern of 1ERR×2ERR, that corresponds to 334.63R$_g$×669.26R_g in the source plane for a black hole mass of $M_{BH} = 10^9 M_\odot$ (Figure 3 left). For numerical reasons, the microlens magnification map is given in pixels, 1000×2000 (1pix=0.33463R$_g$ in source plane). As one can see from Figure 3 (left), the microlensing pattern structures are comparable with a compact X-ray accretion disk.

In our previous investigations based on the straight fold caustic approximation (for more detailed discussion see [8] or [9]), the lack of a correlation between the continuum and Fe Kα line is expected only if the line and X-ray continuum

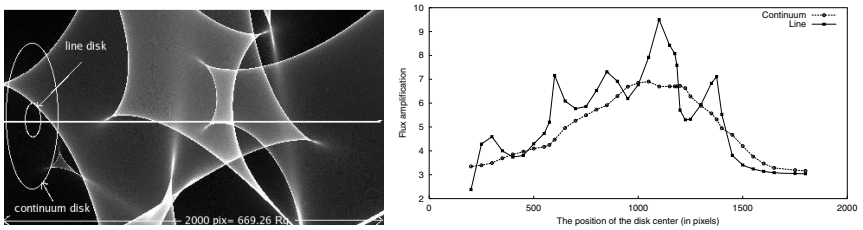

Figure 3. *Left:* microlensing map of QSO 2237+0305A image with 1ERR×2ERR (1000 pix ×2000 pix=334.63 R$_g$×669.26R$_g$) on a side and scheme of the projected disk with outer radius R$_{out}$=20 R$_g$ and 100 R$_g$ for the Fe Kα line and the X-ray continuum, respectively. The straight line presents the path of the center of the disk (left side of the pattern corresponds to 0 pix). *Right:* the amplification of the Fe Kα line and the X-ray continuum total flux for different positions of the disk center on the straight line in the left figure [9].

region are separated. Recent investigations of the Fe Kα line profile from active galaxies show that the line should be emitted from the innermost part of the accretion disk. In particular, in the case of BLRG 4C+74.26 it was found that the outer radius of the relativistic iron line should be within 10 R_g [24]. Consequently, here we will assume that the Fe Kα line is formed in the innermost part of the disk ($R_{\rm inn} = R_{\rm ms}$; $R_{\rm out} = 20$ R_g) and that the continuum (emitted in the energy range between 0.1 keV and 10 keV) is mainly originated from a larger region ($R_{\rm inn} = 20$ R_g; $R_{\rm out} = 100$ R_g). On the other hand, from the straight fold caustic modeling (see [9]) we conclude that the correlation between the total line and continuum flux due to microlensing is not very different for different emissivity laws. Consequently, here we used the black-body emissivity law. A disk (Schwarzschild metric) with an inclination of 35° is considered.

To explore the line and X-ray continuum variation we moved the disk center along the microlensing map shown in Figure 3 (left) from left to the right, i.e. from 0 to 2000 pixels. In Figure 3 (right) we present the corresponding total line and X-ray continuum flux variations. As one can see from Figure 3 (right), there is a global correlation between the total line and continuum flux during the complete path. However, the total continuum flux variation is smooth and has a monotonic change, while the total line flux varies very strongly and randomly.

In fact, during some portion of the microlensing of the emission regions by the magnification pattern, we found the total Fe Kα line flux changes, while the continuum flux remains nearly constant (e.g. the position of the disk center between 1000 and 1200 pixels). This and the shapes of the line and continuum total flux amplification indicate that the observed microlensing amplification of the Fe Kα in three lensed quasars may be explained if the line is originated in the innermost part of the disk and the X-ray continuum in a larger region. Also, it seems that the contribution of the continuum emitted from the innermost part of the disk (within 10 R_g) to the total continuum (in the energy interval from 0.1 to 10 keV) flux is not significant.

4 Conclusions

In order to discuss the observed enhancement of the Fe Kα line in the absence of corresponding continuum amplification found in three lensed QSOs, we developed a model of microlensing of a standard accretion disk by a standard microlensing magnification pattern. Here we summarize several interesting results inferred from our numerical simulations (for more details see [25]).

1. Gravitational microlensing can produce significant variations and amplifications of the line and continuum fluxes of the lensed quasars. These deformations of the X-ray radiation depend on both the disk and microlens parameters.

2. Even microlenses with very small masses could induce significant amplification of the Fe Kα and the X-ray continuum. Thus, the absence of adequate continuum amplification in the observed Fe Kα microlensed QSOs should be related to the structure of the accretion disk and/or the geometry of the event.

3. In the case of microlensing by a standard magnification pattern produced by a population of low mass deflectors, we can successfully reproduce the observed lack of correlation between the X-ray continuum and Fe Kα emission amplification only if the line and continuum emission regions are separated, but only during the limited time intervals, covering the peak of the Fe Kα microlensing event. In that case, microlensing can satisfactorily explain the excess in the iron line emission observed in three gravitational lens systems: MG J0414+0534 [1], QSO 2237+0305 [2] and H 1413+117 [3].

Further observations are needed to provide more data which might be compared with our theoretical results.

Acknowledgments

This work is a part of the project 146002: "Astrophysical Spectroscopy of Extragalactic Objects" supported by the Ministry of Science, Technologies and Development of Serbia.

References

[1] G. Chartas, E. Agol, M. Eracleous, G. Garmire, M.W. Bautz, N.D. Morgan (2002) *ApJ* **568** 509.
[2] X. Dai, G. Chartas, E. Agol, M.W. Bautz, M. W., G.P. Garmire (2003) *ApJ* **589** 100.
[3] G. Chartas, M. Eracleous, E. Agol, S.C. Gallagher (2004) *ApJ* **606** 78.
[4] T. Oshima, K. Mitsuda, R. Fujimoto, N. Iyomoto, K. Futamoto, et al. (2001) *ApJ* **563** L103.
[5] L.Č. Popović, E.G. Mediavilla, P. Jovanović, J.A. Muñoz (2003) *A&A* **398** 975.
[6] K. Nandra, I.M. George, R.F. Mushotzky, T.J. Turner, T. Yaqoob (1997) *ApJ* **477** 602.
[7] A.C. Fabian, S. Vaughan (2003) *MNRAS* **340** L28.
[8] P. Jovanović (2005) *PhD Thesis*, Faculty of Mathematics, University of Belgrade.
[9] L.Č. Popović, P. Jovanović, E.G. Mediavilla, A.F. Zakharov, C. Abajas, J.A. Muñoz, G. Chartas (2006) *ApJ* **637** 620.
[10] K.L. Page, J.N. Reeves, P.T. O'Brien, M.J.L. Turner, D.M. Worrall (2004) *MNRAS* **353** 133.
[11] N.I. Shakura, R.A. Sunyaev (1973) *A&A* **24** 337.

[12] K. Nandra, I.M. George, R.F. Mushotzky, T.J. Turner, T. Yaqoob (1999) *ApJ* **523** 17.

[13] M. Jaroszyński, J.W. Wambsganss, B. Paczyński (1992) *ApJ* **396** L65.

[14] M. Dovčiak, V. Karas, T. Yaqoob (2004) *ApJS* **153**, 205.

[15] L.Č. Popović, P. Jovanović, E.G. Mediavilla, J.A. Muñoz (2003) *Astron. Astrophys. Transactions* **22** 719.

[16] T. Oshima, K. Mitsuda, N. Ota, A. Yonehara, M. Hattori, T. Mihara, Y. Sekimoto (2001) *ApJ* **551** 929.

[17] W. Bian, Y. Zhao (2002) *A&A* **395** 465.

[18] C. Abajas, E.G. Mediavilla, R. Gil-Merino, J.A. Muñoz, J.A., L.Č. Popović, A. Oscoz (2004) presented in IAU 225 Symposium "Impact of Gravitational Lensing on Cosmology", 19-23 July, Lausanne, Switzerland.

[19] C.S. Kochanek (2004) *ApJ* **605** 58.

[20] R. Kayser, S. Refsdal, R. Stabell (1986) *A&A* **166** 36.

[21] P. Schneider, A. Weiss (1987) *A&A* **171** 49.

[22] J. Wambsganss, B. Paczynski, N. Katz (1990) *ApJ* **352** 407.

[23] J. Wambsganss, P. Schneider, B. Paczynski (1990) *ApJ* **358** L33.

[24] D.R. Ballantyne, A.C. Fabian (2005) *ApJ* **622** L97.

[25] P. Jovanović (2006) *PASP* **118** 656.